Deep learning–driven bacterial cytological profiling to determine antimicrobial mechanisms in *Mycobacterium tuberculosis*

Diana Quach[a], Marc Sharp[a] (ID), Sara Ahmed[b], Lauren Ames[b], Amala Bhagwat[b], Aditi Deshpande[b], Tanya Parish[b,c] (ID), Joe Pogliano[d], and Joseph Sugie[a,1] (ID)

Affiliations are included on p. 7.

Tuberculosis (TB), caused by *Mycobacterium tuberculosis*, remains a significant global health threat, affecting an estimated 10.6 million people in 2022. The emergence of multidrug resistant and extensively drug resistant strains necessitates the development of novel and effective drugs. Accelerating the determination of mechanisms of action (MOAs) for these drugs is crucial for advancing TB treatment. This study introduces MycoBCP, a unique adaptation of bacterial cytological profiling (BCP) tailored to *M. tuberculosis*, utilizing the application of convolutional neural networks (CNNs) within BCP to overcome challenges posed by traditional image analysis techniques. Using MycoBCP, we analyzed the morphological effects of various antimicrobial compounds on *M. tuberculosis*, capturing broad patterns rather than relying on precise cell segmentation. This approach circumvented issues such as cell clumping and uneven staining, which are prevalent in *M. tuberculosis*. In a blind test, MycoBCP accurately identified the MOA for 96% of the compounds, with a single misclassification of rifabutin, which was incorrectly categorized as affecting translation rather than transcription. The similar morphologies resulting from transcription and translation inhibition indicate a need for further refinement to distinguish them more effectively. Application of MycoBCP to a series of antitubercular agents successfully identified known MOAs and revealed unique effects, demonstrating its utility in early drug discovery and development. Our findings underscore the potential of CNN-based BCP to enhance the accuracy and efficiency of MOA determination, particularly for challenging pathogens like *M. tuberculosis*. MycoBCP represents a significant advancement in TB drug development, offering a robust and adaptable method for high-throughput screening of antimicrobial compounds.

microbiology | drug discovery | *Mycobacterium tuberculosis* | antimicrobials | convolutional neural networks

Significance

Bacterial cytological profiling (BCP) is a well-established method to determine the mechanism of action (MOA) for antibiotics by examining the morphological changes that occur when bacteria are treated with a compound of interest. This study demonstrates the application of convolutional neural networks (CNN) to overcome technical challenges with a traditional approach to BCP, creating a robust platform to rapidly determine MOA for *Mycobacterium tuberculosis*. We demonstrate the capability of this platform by using it to confirm the MOA of several compounds that target *M. tuberculosis*. Our findings underscore the potential of CNN-based BCP to enhance the accuracy and efficiency of MOA determination, particularly for challenging pathogens like *M. tuberculosis*.

Tuberculosis (TB) is a global health threat caused by *Mycobacterium tuberculosis* (*M. tuberculosis*) that has affected an estimated 10.6 million people in 2022 (1). A 4-mo long regimen of four drugs has been the recommended treatment of susceptible *M. tuberculosis* since 2022 and multidrug resistant (MDR) or extensively drug resistant (XDR) *M. tuberculosis* treatments are longer than 6 mo (1, 2). Novel and effective drugs are urgently needed to fight MDR and XDR *M. tuberculosis* and shorten treatment times. Accelerating mechanism of action (MOA) determination for drugs effective against *M. tuberculosis* has the potential to significantly enhance TB drug development efforts.

A robust microscopy-based method known as bacterial cytological profiling (BCP) has been effectively used to identify MOA for novel antibiotics and crude extracts in various bacterial species (3–8). BCP leverages the observation that inhibition of metabolic pathways induces reproducible changes in cellular architecture. The subsequent differences in morphology can be quantified and profiles corresponding to each metabolic pathway can be characterized (3–8). Compounds with similar MOAs can often be further distinguished based on their unique kinetics or concentration-dependent activity (3–8). To adapt this technology for *M. tuberculosis*, we developed MycoBCP, an imaging and analysis pipeline tailored to this pathogen.

BCP has typically been heavily reliant on accurate cell segmentation and thresholding (3–8). Traditional image analysis tools have been successful in segmenting and measuring cellular properties automatically in bacteria that exhibit minimal cell-to-cell variation and even staining (9–12). Attempts to develop BCP for *M. tuberculosis* using these traditional tools that rely on cell segmentation and individual cell measurements have met with some success (13). However, these approaches, which at a core are based on identifying and measuring single cells, face significant challenges as *M. tuberculosis* tends to clump, exhibit significant cell-to-cell variation, and stain unevenly. All BCP methods benefit from larger

and more varied datasets and such challenges slow data collection and curation. While modern deep learning approaches to cell segmentation have seen large successes (14, 15), here, we introduce a more straightforward solution that has several advantages over segmentation and cell measurement.

Fundamentally, BCP presents an image classification challenge that is ideally suited for convolutional neural networks (CNNs). Instead of isolating and focusing on single cells, morphological differences can be seen as broad patterns in groups of cells—an approach that analyzes images holistically rather than relying entirely on individual cell boundaries. This approach circumvents the difficulties associated with automated image thresholding and cell segmentation which remain particularly problematic in *M. tuberculosis*.

This study introduces MycoBCP, a unique adaptation of BCP tailored to *M. tuberculosis*, that applies CNNs to overcome challenges posed by traditional image analysis techniques. Using the MycoBCP platform, we correctly identified the MOA pathway in 96% (24/25) of compounds in a blind test. Among these, the exact target was identified for 76% (19/25) of the compounds. We then applied MycoBCP to a series of unique antitubercular agents. MycoBCP successfully identified the correct MOA of known compounds (16–21) and revealed effects for some compounds not observed in previous studies, demonstrating its utility in early drug discovery and development.

Methods

Minimum Inhibitory Concentrations (22–24**).** *M. tuberculosis* mc^2 6206 H37Rv Δ*RD1*Δ*panCD* Δ*leuCD* was incubated rolling at 30 °C in Middlebrook 7H9 medium supplemented with 10% Oleic Albumin Dextrose Catalase, 0.5% glycerol, 0.05% Tween 20, 0.2% casamino acids, 48 μg/mL pantothenate, and 50 μg/mL leucine (7H9-PL). Plates for minimum inhibitory concentration (MIC) testing were prepared by making 2× serial dilutions of the compounds in 7H9+PL in round bottom 96-well plates which were then inoculated with a cell culture with the final OD$_{590}$ ~0.02 in a final total volume of 200 μL per well. Growth was often uneven in the perimeter wells of plates, so MICs were confined to the central 60 wells. The plates were incubated at 37 °C without shaking for 7 d, with growth evaluated by eye starting at day 5. The MIC was determined as the first well in a dilution series with no visible growth.

BCP. To prepare cultures for BCP, we diluted a parent *M. tuberculosis* culture grown in 7H9+PL at 30 °C to a final OD$_{600}$ of ~0.06 to 0.08 which was then rolled at 30 °C for 18 to 20 h, a slower growth temperature that provided reproducible phenotypes. After this outgrowth, the culture was split into 2 mL aliquots and treated with sufficient compound to reach the desired test concentration, typically between 1× and 5× the MIC. These treated aliquots were then rolled at 30 °C, and 400 μL samples were harvested and fixed after 48 and 120 h of treatment. Specifically, each 400 μL sample was fixed at 30 °C for 20 min with a mixture of 100 μL of 16% paraformaldehyde, 3 μL of 8% glutaraldehyde, and 20 μL of 0.4 M phosphate buffer, pH 7.5. After fixation, the cells were washed twice with 200 μL of warm 7H9+PL concentrated to a final volume of ~30 μL and stained for 30 min. The cells were stained with 0.04 mg/mL FM 4-64 (Invitrogen), 0.1 to 0.2 mM SYTO 40 (Invitrogen), and 4 μM SYTOX Green (Invitrogen). In images, membranes are shown in red, DNA in blue, and green staining indicates that cell integrity has been compromised; white scale bars are 1 μm.

Image Preparation. Full-field fluorescence microcopy images of samples prepared for BCP are preprocessed from their original proprietary microscope file format to Tagged Image File Format. The original image dimensions 3 × 2,048 × 2,048 are cropped to 3 × 1,800 × 1,800 by trimming 124 pixels from each edge to avoid optical artifacts. Each image is divided into nine subimages of dimensions 3 × 600 × 600. Image entropy [calculated as sum(p*log2(p)] where p is the normalized histogram counts) is used to automatically filter out images without a significant number of cells. A total of 46,052 subimages were used to train the CNN (*SI Appendix*, Tables S3 and S4).

For testing, a 600 pixel square sliding window is passed over the trimmed image using a step size of 60 pixels to create 400 subimages which are each passed to the trained CNN and produce a vector denoting a point in a latent space. Similarity scores are calculated by relating the location of unknown compound treated cells in this space to control compound treated cells using a scaled version of the average minimum distance.

Results

Antibacterial Treatment Produces Distinct Phenotypes in *M. tuberculosis*. To create a platform capable of classifying the MOA for potential antimicrobial agents, we conducted a series of experiments aimed at distinguishing between distinct phenotypes induced by treatment in *M. tuberculosis*. Following on previous work in BCP (3–8), we treated *M. tuberculosis* grown in 7H9+PL with drug concentrations between 1× and 5× the MIC for 48 and 120 h. We fixed these samples, stained them using FM 4-64, SYTO 40, and SYTOX Green and imaged them with high-resolution fluorescence microscopy. We observed distinct phenotypes in treated *M. tuberculosis* cells; however, unlike our previous work in BCP, morphological differences were subtle and required a high precision in cell segmentation and measurement to meaningfully classify MOAs. Traditional BCP methods, which involve segmenting cells and quantifying cellular properties such as cell length, cell area, and intensity, are well suited to organisms such as *Escherichia coli* and *Acinetobacter baumannii* (Fig. 1*A*). These cells exhibit uniform membrane and DNA staining that facilitates segmentation and measurement. Furthermore, most pathways in *E. coli* and *A. baumannii* produce distinct morphologies that can be characterized by critical features, such as the formation of toroidal DNA in compounds targeting translation (4, 8) (Fig. 1*A*). In comparison, *M. tuberculosis* has a propensity to clump, stains poorly, and generally does not display singular morphological features that are wholly unique to individual pathways. Thus, we adapted BCP to utilize neural networks which enabled us to capture broader, multicellular patterns and remove our reliance on precise thresholding and cell segmentation. In this way, we can de-emphasize common features and look for combinations of atypical features that can accurately discriminate MOA, thereby enhancing the accuracy of classification even when visual cues were less pronounced. The kinetics of each compound can vary greatly, necessitating multiple observations to capture the evolution of certain morphologies. Therefore, data were collected at two time points: 48 h and 120 h posttreatment.

CNN. The primary obstacle in employing CNNs for BCP lies in the need to amass extensive, highly specialized datasets—a crucial step to effectively train a network that is both generalizable and not prone to overfitting (25, 26). Here, we selected 23 antimicrobials to represent a wide range of pathways, producing a collection of over 5,000 images which were preprocessed into 46,052 subimages as outlined in the "*Methods: Image Preparation.*" The CNN was initially trained on this dataset as a classifier for MOA groups. We then removed the softmax activation layer to utilize the CNN as an encoder that takes images and outputs values from the final fully connected layer (Fig. 1 *B* and *C* and *SI Appendix*, Tables S3 and S4).

To facilitate the rapid addition and evaluation of compounds beyond the initial set of 23 used for training, we compiled an independent dataset of control compounds, termed the "feature set," as shown in Fig. 1*B*. This feature set was processed by the CNN, which encoded the data into the latent space, allowing us to represent each compound as a cluster of points in this space. The encoded information is then utilized to assess compound similarity through the calculation of the average minimum
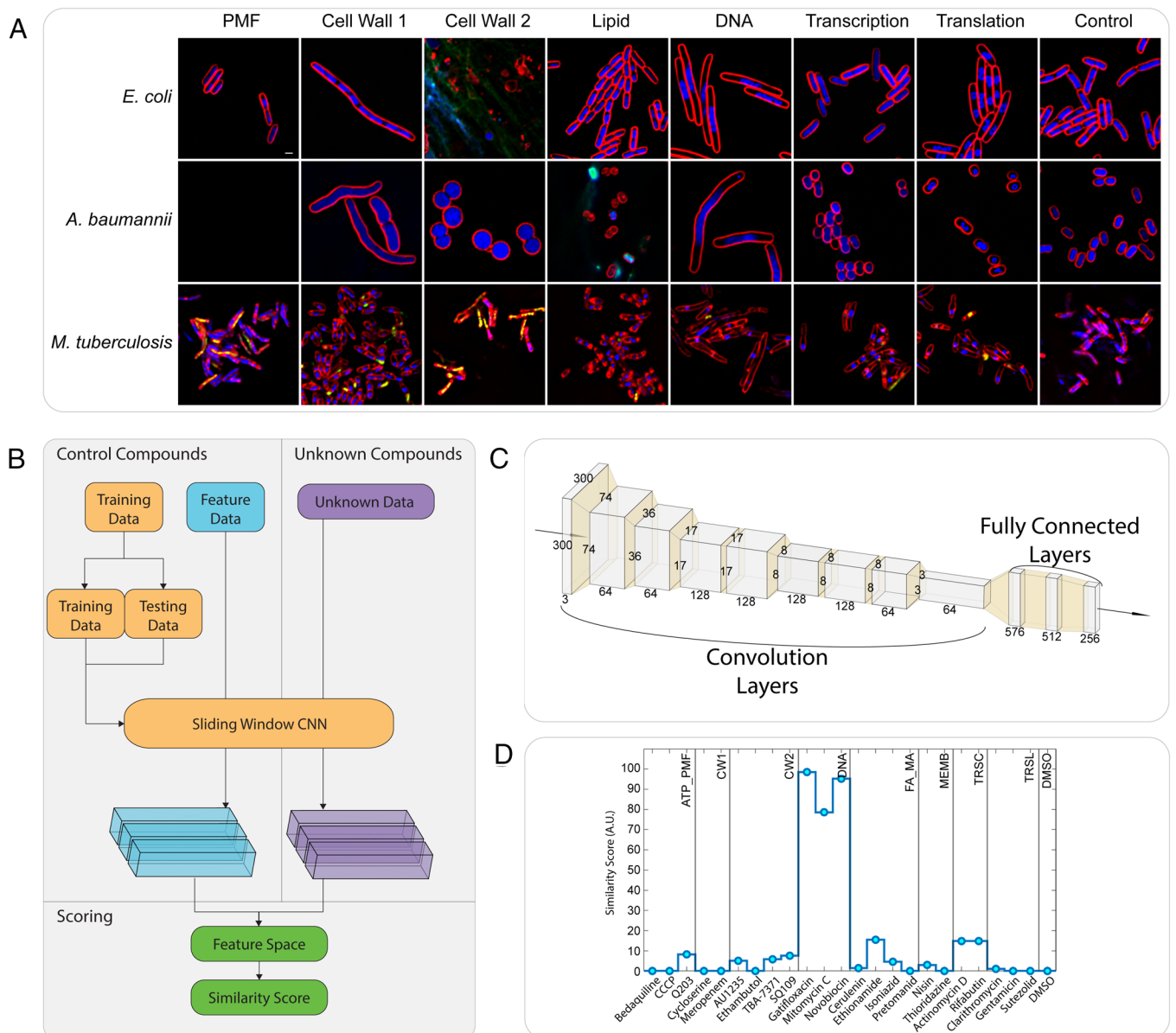
Fig. 1. (*A*) *E. coli*, *A baumannii*, and *M. tuberculosis* cells treated with compounds affecting different pathways. Membranes are red (FM 4-64), DNA is blue (SYTO 40), and membrane permeability is green (SYTOX Green). Scale bar is 1 μm. (*B*) Model architecture. Arrows show the information flow among different components. Training data (orange) is used to train the CNN. Feature data (blue) are used with the trained CNN as an encoder to map out areas of a feature space with known MOAs. Cells treated with unknown compounds (purple) are processed similarly to feature data and MOA is evaluated based on similarity to feature data as represented by a similarity score. (*C*) CNN model architecture describing the shape of each convolution and fully connected layer. (*D*) Similarity scores for gatifloxacin-treated cells compared to all control compounds sorted by MOA pathway.

distance between points representing different compounds. We scale this metric from 0 to 100 and plot similarity to all control compounds to provide a clear, intuitive visualization of compound similarity based on their MOA (Fig. 1*D*). For example, cells treated with Gatifloxacin produce high similarity scores to control cells treated with a variety of DNA replication inhibitors and low scores against compounds affecting other pathways (Fig. 1*D*). Notably, some control compounds exhibit phenotypes that are indistinguishable; hence, we categorize these compounds into groups that approximately reflect the pathways they affect, as detailed in *SI Appendix*, Table S1.

Blind Test. To assess the reliability of our platform, we conducted a blind test using our full set of 23 control compounds and two samples of dimethyl sulfoxide, which served as negative controls. A fresh set of images, collected independently from those used in

the training and feature sets, was used for this evaluation (Fig. 2). The compounds were classified without prior knowledge of their identities to simulate a realistic application scenario. The average maximum similarity score in this test was 90.69 ± 6.93, indicating a high level of reproducibility and confidence in matching to the controls.

Our platform successfully identified the correct MOA for 96% of the samples, accurately classifying 24 out of the 25 compounds (Fig. 2). The sole misclassification involved rifabutin, which was incorrectly predicted to impact the translation pathway rather than its categorized target, transcription. To determine whether this was an isolated case or indicative of a broader issue with rifamycins, we conducted additional unblinded tests with rifampicin and rifapentine. Both compounds were correctly classified as transcription inhibitors (*SI Appendix*, Fig. S5) suggesting no specific issue in the determination of rifamycin MOAs.
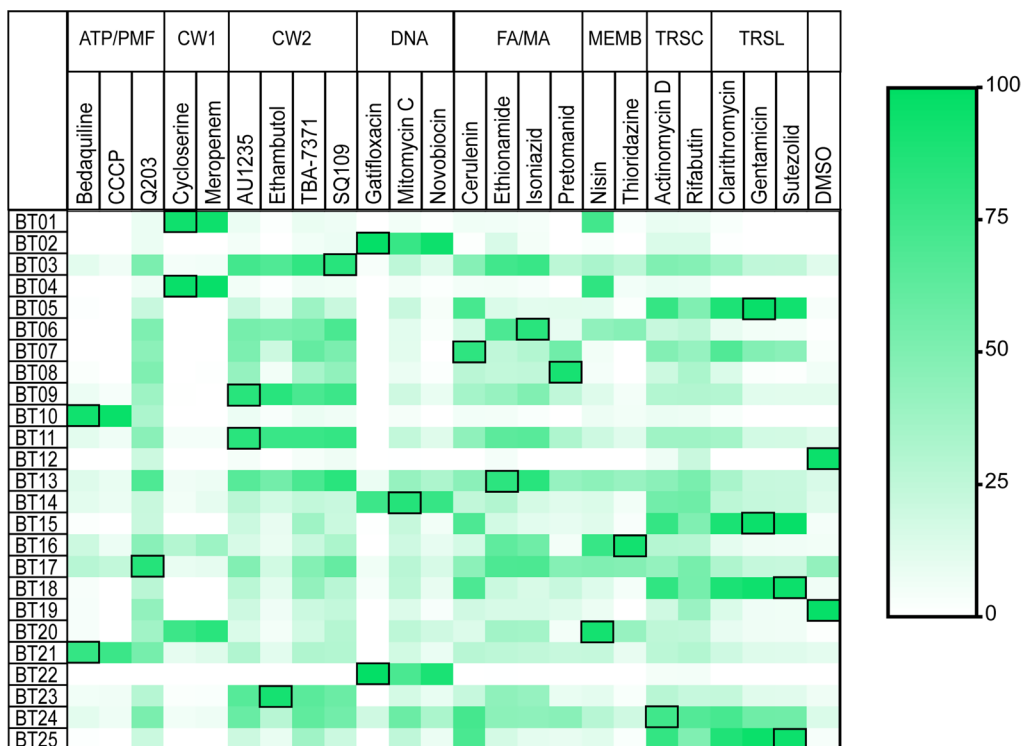
Fig. 2. Similarity matrix for blinded compounds compared to control compounds. High similarity scores are green and low are white. The highest similarity score for each blinded compound is highlighted with a black box.

Furthermore, 19 out of the 25 compounds (76%) were matched to the exact same compound in the control group, demonstrating the platform's potential ability to discern differences within the established MOA pathways.

MOA and Compound Similarities. BCP technology operates by correlating specific morphologies with their respective cellular targets (3–8). In an ideal scenario, compounds targeting the same cellular function should exhibit identical morphologies and thus be classified similarly. This principle also extends to our control antimicrobials, many of which target similar pathways or points along the same pathway. Thus, we aimed to evaluate the distinctiveness of individual pathways. Fig. 3 illustrates the similarity among our control antimicrobials at the different points of 48 (Fig. 3A) and 120 h (Fig. 3B), with green indicating similarity and white denoting dissimilarity. Bright green squares along the main diagonal suggest high similarity, indicating compounds that group together. The significant high-similarity areas align well with the groups into which we organized these compounds based on their targets. Average similarity score for a control to those within its MOA group was 82.3 whereas the similarity to controls outside the MOA group was an average of 28.2.

Notably, similarity regions outside the main diagonal suggest potential misclassifications between targets. For example, the group of compounds affecting fatty acid or mycolic acid pathways (FA/MA) shows high similarity to the cell wall group 2 (CW2; MmpL3/arabinogalactan inhibitors) at 48 h (Fig. 3A). While metabolically plausible, since FA/MA targets are upstream of CW2 targets, this suggests that a 48-h observation alone is inadequate for distinguishing these groups. However, by 120 h, this similarity largely vanishes (Fig. 3B), supporting the need for multiple time points.

We chose 48 h to capture early morphological changes, particularly for rapidly acting compounds like membrane disruptors, and 120 h to observe later-developing changes that provide

distinguishable morphologies for most control compounds. To underscore changes occurring between these two time points, we plotted the difference between similarity scores (Fig. 3C). Red indicates decreasing similarity over time, whereas green denotes emerging similarities by 120 h that were not evident at 48 h. This highlights pathways where data from 48 h may be more discriminative, and instances where observations at 120 h are crucial, reinforcing the necessity of multiple time points for accurate classification. While cells treated with transcription and translation inhibitors generate similar images and produce related similarity scores, the platform currently identified 4 out of 5 transcription and translation inhibitors (Fig. 2).

Antitubercular Agents. We have previously identified many molecules with activity against *M. tuberculosis* in aerobic culture (16–21). We selected eight of these which represented classes with known targets or with targets which were predicted from studies with resistant mutants. Compounds were tested blinded to avoid bias in interpretation and the identity of molecules were revealed after the mode of action prediction. We tested these using the MycoBCP platform, to determine how effectively it identifies MOAs outside our standard control library. Imaging *M. tuberculosis* after treatment with these compounds revealed distinct MOAs for each compound that grouped into two sets (Fig. 4A). We found that, using the concentrations and time points tested, the MycoBCP platform correctly identified the MOA for these two unique sets of compounds.

One set of compounds (TPN-0001046, TPN-0001390, TPN-0091218) induced morphological changes indicative of impacts on the cell wall and were predicted to target the arabino-galactan biosynthesis and lipid transporter protein MmpL3 (Fig. 4 and *SI Appendix*, Fig. S3). This set of compounds contained a known MmpL3 inhibitor (AU1235) as well as aryl indoles that we previously identified as MmpL3 inhibitors based on their loss of activity against strains with mutations in MmpL3 (21). The
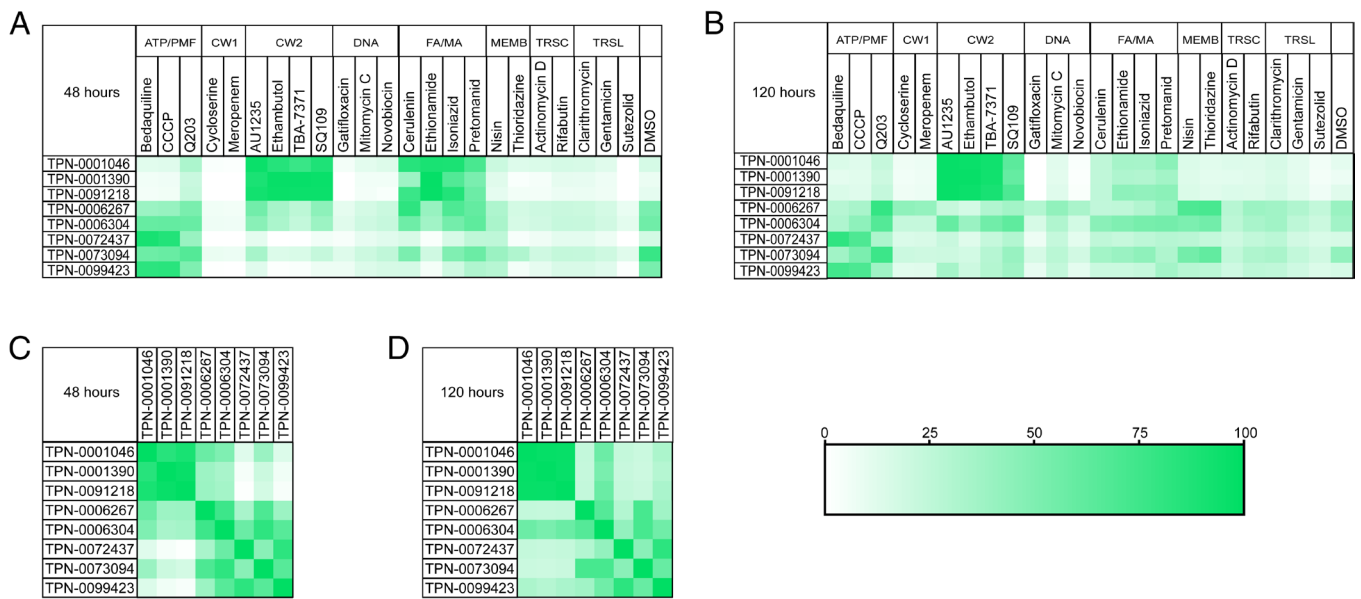
Fig. 3. (*A*) Similarity matrix for control compounds using data at 48 h of treatment. A maximum similarity score of 100 is represented by green and a minimum similarity score of 0 is white. (*B*) Similarity matrix for control compounds using data at 120 h of treatment with the same color representation as in *A*. (*C*) Difference between similarity scores at 120 h of treatment and 48 h of treatment. A positive difference of 100 is represented by green and a negative difference of −100 is represented by red. Green shows a higher similarity between compounds developing at 120 h, whereas red shows a lower similarity between compounds at 120 h.

platform was able to correctly identify both known and suspected MmpL3 inhibitors.

The second set of compounds, TPN-0006267, TPN-0006304, TPN-0072437, TPN-0073094, and TPN-0099423, were categorized as adenosine triphosphate synthase/proton motive force (ATP/PMF) inhibitors by the CNN. This set included known inhibitors of the cytochrome bc1 complex (QcrB) and spanned multiple chemical classes: Azabenzimidazoles, Triazolopyrimidines, Morpholinobenzamides, and Imidazopyridines (16–20). While the MmpL3 inhibitors produced cells with a distinctive morphology and very high similarity scores, the QcrB inhibitors presented more subtle morphological changes and were sensitive to the kinetics of

treatment resulting in lower similarity scores within the group (Fig. 4 *C* and *D*). Previous research (16, 17) suggests that these QcrB inhibitors exhibit similar activity, raising intriguing questions about potential heterogeneity within these series.

Discussion

CNN and Feature Space. Targeting specific pathways in *M. tuberculosis* leads to reproducible physical changes in cells, a key observation that enables BCP to discriminate and identify MOA. Previous work with Gram-negative and Gram-positive bacteria has successfully utilized traditional image analysis techniques for BCP,

Fig. 4. (A) Similarity matrix for antitubercular compounds compared to control compounds at 48 h of treatment. High similarity scores are green and low are white. (B) Similarity matrix for antitubercular compounds compared to control compounds at 120 h of treatment. (C) Similarity matrix for antitubercular compounds compared against themselves at 48 h of treatment. (D) Similarity matrix for antitubercular compounds compared against themselves at 120 h of treatment.

involving thresholding, segmentation, and measurement to extract physical features such as cell length, width, area, and perimeter (3–8). These features provide meaningful biological insights into the effects of various antimicrobial compounds. While the phenotypes of bacteria such as *E. coli* treated with different compounds are so distinctive that AI approaches are not necessary for classification (4), such an approach has an advantage of increasing throughput and automation.

In this study, we explored the use of a CNN as an encoder to replace the tasks of thresholding, segmentation, and measurement traditionally required in BCP in order to study a bacterium where the phenotypes are less distinct. Instead of directly classifying images, the CNN encodes each image into a latent space, resulting in a set of values that serve as a comprehensive representation of the morphological changes induced by different compounds. This latent space encoding allows us to capture subtle and complex patterns in *M. tuberculosis* cell morphology that may be missed by conventional methods. By employing the CNN as an encoder, we gain several significant advantages. First, this approach bypasses the challenges associated with precise cell segmentation and measurement, which are particularly problematic for *M. tuberculosis* due to its tendency to clump and stain unevenly. Second, the latent space generated by the CNN provides a flexible framework for analyzing new compounds. We can add new compounds to our control set and compare them within this latent space without the need for retraining the network each time a new compound is introduced. This flexibility is critical as no set of curated control compounds would be comprehensive enough to cover every possible target. Our findings suggest that the use of CNNs in BCP can significantly enhance the accuracy and efficiency of MOA determination, particularly for challenging pathogens like *M. tuberculosis*. Integrating modern machine learning approaches into BCP represents a significant advancement in the field of BCP, offering a more adaptable and precise method for MOA identification.

Blind Test. Our platform accurately identified the MOA for 96% of the compounds in a blind test. The sole misclassification involved rifabutin, which was incorrectly categorized as affecting

the translation pathway instead of its actual target, the transcription pathway. A detailed analysis of our controls (Fig. 3 *A* and *B*) revealed regions where treated cells exhibited high similarity between compounds classified under translation and transcription. Despite the correct classification of rifampicin and rifapentine (*SI Appendix*, Fig. S5), the misclassification of rifabutin highlights a challenge in differentiating between certain compounds in *M. tuberculosis*. While compounds targeting these pathways are easily distinguished between in *E. coli*, they result in overlapping morphological phenotypes in *M. tuberculosis*, making it difficult for the CNN to identify discriminating features between these specific MOAs. This observation underscores the importance of further refining our profiling methods to enhance the resolution between these two pathways.

Future investigations will focus on expanding our training data to include a wider variety of targets, aiming to improve generalizability to new compounds. The high rate of matching to not only the correct pathway but also to the identity of the control compounds in our blind test may be influenced by the inclusion of the same compounds in both the training and test sets. However, because the data were collected entirely independently, this suggests that there may be potential to further separate compounds in even closely related pathways. Despite this limitation, our platform's overall accuracy demonstrates its robustness and potential for high-throughput MOA determination in TB drug development. The ability to accurately classify MOA for 96% of the compounds and match 76% to the exact control compound underscores the effectiveness of MycoBCP in discerning subtle differences in MOA.

MycoBCP clearly identified known and suspected MmpL3 inhibitors as a distinct class with specific morphological changes. The patterns were distinct from other cell wall inhibitors and raise the possibility of using MycoBCP to rapidly identify new MmpL3 inhibitors, as well as monitor for target drift during the hit-to-lead and lead optimization phases of drug discovery. MycoBCP also confirmed that the mode of action of compounds suspected to be QcrB inhibitors do indeed disrupt respiration as expected and raised biological questions about these compounds. The heterogeneity of the response, indicated by their low similarity scores to each other,

in the QcrB inhibitors was intriguing and suggests that there are different subpopulations of bacteria with differing sensitivities to inhibition of respiration, even during aerobic growth. Since QcrB inhibitors are largely bacteriostatic against replicating bacilli, but bactericidal against non-replicating (nutrient-starved) bacteria, this might be due to bacteria being in different physiological states.

Combining deep learning and BCP has shown significant advantages over traditional cell segmentation and measurement. Properly thresholding cells to get good segmentation often relies on even staining of cell membranes and spacing of cells. Poor staining leads to unclear cell borders while the clumping of cells creates problems with the accurate determination of the correct focal plane. A common approach is to filter out cells that are not recognized by a segmentation algorithm, but this leads to a systematic loss of information from clumped and poorly stained cells. Less automated measurements can fix this but are time-consuming and can be a major barrier to adding new data to a platform. Additionally, once segmented, striking a balance in feature selection to retain generality while striving for accuracy can be difficult with an abundance of features to measure.

Utilizing CNNs as encoders eliminates these issues at the cost of requiring more data. While traditional BCP methods can be built on a handful of microscopy images, getting meaningful results from neural networks can require tens to hundreds of thousands of datapoints. In exchange, CNNs are rapid, can be integrated into a fully automated pipeline, and can utilize information from both intra- and intercellular sources. By using a CNN as an encoder and not incorporating a classifier, we can quickly add new data for comparison to our feature space without the need to retrain. As BCP platforms become more widespread and more data are accumulated, deep learning approaches will begin to see more use.

Author affiliations: [a]Linnaeus Bioscience, Inc., San Diego, CA 92109; [b]Center for Global Infectious Disease Research, Seattle Children's Research Institute, Seattle, WA 98109; [c]Department of Pediatrics, University of Washington School of Medicine, Seattle, WA 98109; and [d]Department of Molecular Biology, University of California, San Diego, CA 92093

1. World Health Organization, *Global tuberculosis report 2023* (World Health Organization, Geneva, Switzerland, 2023).
2. World Health Organization, *WHO consolidated guidelines on tuberculosis: Module 4: Treatment: drug-susceptible tuberculosis treatment* (World Health Organization, Geneva, Switzerland, 2022).
3. A. Lamsa, W.-T. Liu, P. C. Dorrestein, K. Pogliano, The Bacillus subtilis cannibalism toxin SDP collapses the proton motive force and induces autolysis. *Mol. Microbiol.* **84**, 486–500 (2012).
4. P. Nonejuie, M. Burkart, K. Pogliano, J. Pogliano, Bacterial cytological profiling rapidly identifies the cellular pathways targeted by antibacterial molecules. *Proc. Natl. Acad. Sci. U.S.A.* **110**, 16169–16174 (2013).
5. D. T. Quach, G. Sakoulas, V. Nizet, J. Pogliano, K. Pogliano, Bacterial Cytological Profiling (BCP) as a rapid and accurate antimicrobial susceptibility testing method for Staphylococcus aureus. *EBioMedicine* **4**, 95–103 (2016).
6. P. Nonejuie *et al.*, Application of bacterial cytological profiling to crude natural product extracts reveals the antibacterial arsenal of Bacillus subtilis. *J. Antibiot. (Tokyo)* **69**, 353–361 (2016).
7. A. Lamsa *et al.*, Rapid inhibition profiling in Bacillus subtilis to identify the mechanism of action of new antimicrobials. *ACS Chem. Biol.* **11**, 2222–2231 (2016).
8. H. H. Htoo *et al.*, Bacterial cytological profiling as a tool to study mechanisms of action of antibiotics that are active against Acinetobacter baumannii. *Antimicrob. Agents Chemother.* **63**, e02310-18 (2019), 10.1128/aac.02310-18.
9. S. Stylianidou, C. Brennan, S. B. Nissen, N. J. Kuwada, P. A. Wiggins, SuperSegger: Robust image segmentation, analysis and lineage tracking of bacterial cells. *Mol. Microbiol.* **102**, 690–700 (2016).
10. A. Paintdakhi *et al.*, Oufti: An integrated software package for high-accuracy, high-throughput quantitative microscopy analysis. *Mol. Microbiol.* **99**, 767–777 (2016).
11. T. Ursell *et al.*, Rapid, precise quantification of bacterial cellular dimensions across a genomic-scale knockout library. *BMC Biol.* **15**, 17 (2017).
12. C. McQuin *et al.*, Cell Profiler 3.0: Next-generation image processing for biology. *PLoS Biol.* **16**, e2005970 (2018).
13. T. C. Smith *et al.*, Morphological profiling of tubercle bacilli identifies drug pathways of action. *Proc. Natl. Acad. Sci. U.S.A.* **117**, 18744–18753 (2020).
14. E. Moen *et al.*, Deep learning for cellular image analysis. *Nat. Methods* **16**, 1233–1246 (2019).
15. A. Zagajewski *et al.*, Deep learning and single-cell phenotyping for rapid antimicrobial susceptibility detection in Escherichia coli. *Commun. Biol.* **6**, 1–12 (2023).
16. C. Shelton *et al.*, Triazolopyrimidines target aerobic respiration in Mycobacterium tuberculosis. *Antimicrob. Agents Chemother.* **66**, e0204121 (2022).
17. L. A. T. Cleghorn *et al.*, Identification of morpholino thiophenes as novel Mycobacterium tuberculosis inhibitors, targeting QcrB. *J. Med. Chem.* **61**, 6592–6608 (2018).
18. E. S. Zuniga *et al.*, The synthesis and evaluation of triazolopyrimidines as anti-tubercular agents. *Bioorg. Med. Chem.* **25**, 3922–3946 (2017).
19. K. A. Abrahams *et al.*, Identification of novel imidazo[1,2-a]pyridine inhibitors targeting M. tuberculosis QcrB. *PLoS One* **7**, e52951 (2012).
20. T. O'Malley *et al.*, Imidazopyridine compounds inhibit mycobacterial growth by depleting ATP levels. *Antimicrob. Agents Chemother.* **62**, e02439-17 (2018), 10.1128/aac.02439-17.
21. M. B. McNeil *et al.*, Multiple mutations in Mycobacterium tuberculosis MmpL3 increase resistance to MmpL3 inhibitors. *mSphere* **5**, e00985-20 (2020), 10.1128/msphere.00985-20.
22. J. Ollinger *et al.*, A dual read-out assay to evaluate the potency of compounds active against Mycobacterium tuberculosis. *PLoS One* **8**, e60531 (2013).
23. J. V. Early, S. Mullen, T. Parish, A rapid, low pH, nutrient stress, assay to determine the bactericidal activity of compounds against non-replicating Mycobacterium tuberculosis. *PLoS One* **14**, e0222970 (2019).
24. J. Ollinger *et al.*, A high-throughput whole cell screen to identify inhibitors of Mycobacterium tuberculosis. *PLoS One* **14**, e0205479 (2019).
25. A. Krizhevsky, I. Sutskever, G. Hinton, ImageNet classification with deep convolutional neural networks. *Commun. ACM* **60**, 84–90 (2017).
26. K. O'Shea, R. Nash, An introduction to convolutional neural networks. arXiv [Preprint] (2015). https://doi.org/10.48550/arXiv.1511.08458 (Accessed 17 May 2024).
27. J. Sugie, MycoBCP sample code. GitHub. https://github.com/MycoBCP/MycoBCP. Deposited 16 September 2024.